International Communications in Heat and Mass Transfer 110 (2020) 104433

Contents lists available at ScienceDirect

International Communications in Heat and Mass Transfer

journal homepage: www.elsevier.com/locate/ichmt

Transient thermo-hydraulics and performance characteristics of single-phase natural circulation loop using hybrid nanofluids

Mayaram Sahu, Jahar Sarkar*, Laltu Chandra

Department of Mechanical Engineering, Indian Institute of Technology (B.H.U.), Varanasi, UP 221005, India

ARTICLE INFO

Keywords:
Single-phase natural circulation
Hybrid nanofluids
Nanoparticle shape
Stability
Mass flow rate
Entropy generation

ABSTRACT

Transient analysis of vertical heating and horizontal cooling rectangular single-phase natural circulation loop with various water-based hybrid nanofluids (Al_2O_3 + Ag, Al_2O_3 + Cu, Al_2O_3 + TiO_2, Al_2O_3 + CNT, Al_2O_3 + Graphene) with 1% volumetric concentration is studied numerically. Temporal fluctuation and time required to attain the steady-state, transient mass flow rate and energy-exergy performance parameters (effectiveness and total entropy generation) using hybrid nanofluids are compared with water. The effect of power input and geometry parameter (diameter and height) of the loop on transient performances is studied as well. The result reveals that the fluctuation of mass flow rate and time required to attain the steady-state are less for hybrid nanofluids as compared to water. However, platelet and cylindrical shaped nanoparticles yield a lower stability as compared to spherical shaped. The mass flow rate is enhanced with hybrid nanofluids, except Al_2O_3 + CNT and Al_2O_3 + Graphene, as compared to water. The energy-exergy performance of hybrid nanofluids is higher than water. The maximum increment in mass flow rate is shown by Al_2O_3 + Ag hybrid nanofluid (3%), whereas Al_2O_3 + Graphene shows the highest increment in effectiveness (25.4%) and highest decrement in total entropy generation (14.3%) as compared to water. Smaller diameter and lower height of loop are found preferable for the flow stability.

1. Introduction

Natural Circulation Loop (NCL) offers an efficient choice as a heat transfer device since it works due to the favorable density gradient developed between the source (heater) and sink (cooler) without any aid of external power [1,2]. However, the associated inherent disadvantages are the low mass flow rate and the related flow instability or reversal that remains a major challenge for its practical implementation. Numerous numerical and experimental studies have been performed to understand the dynamic behavior and stability of NCL. Welander [3] theoretically described the mechanism that triggers flow instability in a loop with a point heat source located at the top and a point heat sink located at the bottom. The first experiment was performed by Creveling et al. [4] to analyze the flow instability and/or reversal in a toroidal shaped water loop and reported the flow stability at a low or high heat transfer rate. Chen [5] theoretically showed that the aspect ratio of a loop (height/width) has a significant influence on flow stability in single-phase NCL (SPNCL) and found the least stable as aspect ratio approaches to unity. Vijayan [6] developed a correlation of Reynolds number in terms of a non-dimensional parameter, which predicts the steady-state flow behavior with uniform and non-uniform loop diameter. Mousavian et al. [7] performed a numerical simulation using RELAP5 system code of HHHC rectangular SPNCL to analyze the transient and stability behaviour of the loop. Vijayan et al. [8] experimentally studied the effect of loop diameter on the flow stability of NCL and found that decreasing the loop diameter enhances the stability. Rao et al. [9] numerically investigated the dynamic response of SPNCL with end heat exchangers for various excitations such as sinusoidal, step, exponential and ramp excitations. Basu et al. [10] analyzed the influence of loop shape on the stability of the SPNCL and found that the rectangular loop is less stable than the toroidal loop. Basu et al. [11] studied the dynamic behavior of rectangular NCL on the different nature of heat input excitations and found that modified exponential excitation is best for increasing or decreasing power input. Devia and Misale [12] performed numerical and experimental investigations on the thermo-hydraulic behaviour of HHHC based SPNCL for the different heat sink temperatures. The effect of constant and variable power inputs on the thermo-hydraulic behaviour of rectangular SPNCL is

Abbreviations: NCL, Natural circulation loop; SPNCL, Single Phase NCL; TR, Temperature ratio; VHVC, Vertical heating vertical cooling; VHHC, Vertical heating horizontal cooling; HHHC, Horizontal heating horizontal cooling

* Corresponding author.
E-mail address: jsarkar.mec@itbhu.ac.in (J. Sarkar).

https://doi.org/10.1016/j.icheatmasstransfer.2019.104433

Available online 09 December 2019

Nomenclature

A	Area of cross-section, m^2
C_p	Specific heat, J/kg-K
d	diameter of the loop, m
f	Friction factor
g	Acceleration due to gravity, m/s^2
h	Heat transfer coefficient, W/m^2-K
H	Height of the loop, m
k	Thermal conductivity, W/m-K
L	Loop width, m
L_C	length of cooler, m
L_H	length of heater (m)
L_t	Total loop length, m
$\dot{m}$	Mass flow rate, kg/s
P	Pressure, N/m^2
Pr	Prandtl number
Q	Heat input rate, W
s	Space coordinate, m
t	Time, s
T	Temperature, K

Greek symbols

α	Thermal diffusivity, m^2/s
β	Coefficient of thermal expansion, 1/K
μ	Dynamic viscosity, N-s/m^2
ϕ	Volume concentration of nanoparticles
ρ	Density of fluid, kg/m^3
ψ	Sphericity
ε	Effectiveness

Subscripts

0	References state
f	Base fluid
in	Inlet
hnf	Hybrid Nanofluid
out	Outlet
p	Nanoparticle

investigated experimentally by Misale [13]. Luzzi et al. [14] developed a semi-analytical expression and a numerical model to predict the dynamic behaviour of SPNCL loop incorporating thermal inertia of the piping material and found a good agreement with the experimental result. Cammi et al. [15] proposed information entropy-based approach to study the dynamic response of SPNCL for generating the stability map of the system. Marchitto and Misale [16] experimentally investigated the thermal performance of a single and two rectangular loops in parallel with different heater powers and sink temperatures. Srivastava et al. [17] experimentally studied the dynamic response of NCL with molten salt for reactor cooling for different heater inputs. Krishnani and Basu [18] studied the influence of heater power, sink temperature and loop inclination on the stability of the system and found that the instability increases with increasing heater power and sink temperature and decreases with increasing loop inclination.

As the reasons behind the instability behavior of SPNCL are exposed, the researchers are attracted towards the problem and are making an effort to control the instability behavior of NCL. Misale and Frogheri [19] experimental studied the influence of the different sizes of the orifice on the stability response of NCL. All the orifices showed stable response with a decrease in mass flow rate because of increased pressure drop. The effect of orientation of the source and sink on the stability in a rectangular single-phase NCL has been experimentally studied by Vijayan et al. [20] and found that the loop is most stable for orientation having VHVC and least stable for HHHC. Misale et al. [21] studied experimentally the dynamic response of NCL by varying the sink temperature and found that stability can be attained by decreasing the sink temperature without changing heater power. This may not practically feasible as it is restricted by ambient temperature. The stability is achieved at the expense of increasing the pressure drop which reduces the mass flow rate or economically infeasible. Nanofluid has been recently proposed as a stabilized agent. Nayak et al. [22,23] experimentally studied the stability behavior of nanofluids in a rectangular single-phase NCL and found significantly enhanced mass flow rate and stability. Misale et al. [24] investigated experimentally the influence of sink temperature and loop inclination on the thermal performance of mini NCL with Al_2O_3/water nanofluid. Ho et al. [25] did not find any significant reduction in resistance by using Al_2O_3 nanofluid in NCL with microchannel source and sink. Dogana and Turgut [26] and Koca et al. [27] experimentally studied the thermal performance of single-phase NCL with Al_2O_3/water and Ag/water nanofluid, respectively. Both concluded that effectiveness factor increases with particle concentration. Devi et al. [28] theoretically found 4% reduction in NCL size by using Fe_3O_4/water nanofluid at 1% concentration as compared to water. Thomas and Sobhan [29] experimentally studied the steady-state and transient behavior of rectangular NCL using nanofluids and found superior heat transfer ability compared to water.

Studies on NCL using nanofluids are limited for metal and ceramic nanoparticles only and reported enhanced mass flow rate and stability. Now the question is whether it is true for all types of nanoparticles. With the best of the author's knowledge, the transient behavior of hybrid nanofluids in NCL with different nanoparticle morphology is unexplored. Therefore, in the present study, the effects of using hybrid nanofluids with different types (different shape and nature) of nanoparticle combinations on the transient behavior of VHHC rectangular single-phase NCL are studied. The effect of power input and geometric parameter (diameter and height) on the mass flow rate, thermal performance parameter and entropy generation under transient and steady-state conditions has been studied.

2. Mathematical modeling and simulation

Rectangular VHHC SPNCL considered in this study consists of a heater, cooler, hot leg and cold leg as shown in Fig. 1. A constant heat flux boundary condition is applied at the heater and a constant wall temperature is imposed on the cooler section of the loop. Constant wall temperature can be considered by supplying a sufficient coolant flow rate (temperature variation of coolant < 1 °C). The cooler is modeled as a counter-flow type heat exchanger for simplicity. The loop is externally insulated except the heating and cooling sections for the obvious reason. The hybrid nanofluids/water is used as the primary fluid and water as the coolant or secondary fluid. The temperature-dependent thermo-properties of primary fluid are assumed to be constant except the density. The coolant temperature is set as the reference low temperature in the NCL. Following assumptions are employed for one-dimensional analysis of the flow in this loop:

(i) The effect of axial conduction and viscous dissipation are ignored.
(ii) The Boussinesq approximation has been used with density varying linearly with temperature as $\rho = \rho_0[1 - \beta_{avg}(T - T_0)]$.
(iii) Minor and heat losses are ignored.

2.1. Governing equations

This section presents the simplified governing equations for the primary fluid as follows:

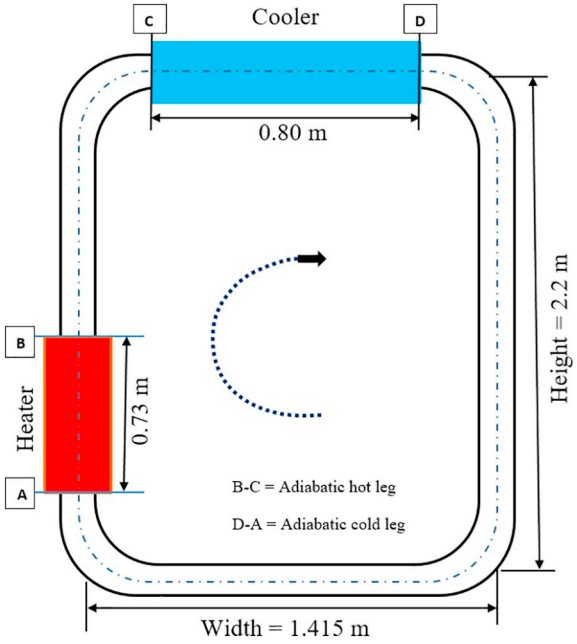

Fig. 1. Schematic diagram of rectangular VHHC single phase NCL.

Continuity:

$$\frac{\partial \dot{m}}{\partial s} = 0 \tag{1}$$

This equation represents the spatial invariance of the mass flow rate. The conservation of momentum is given by,

$$\frac{1}{A}\frac{\partial \dot{m}}{\partial t} + \frac{1}{\rho_o A^2}\frac{\partial \dot{m}^2}{\partial s} = -\frac{\partial P}{\partial s} - \rho g \cos\theta - \frac{f\dot{m}^2}{2d\rho_o A^2} \tag{2}$$

Integration of Eq. (2) around the closed loop with $\oint dp = 0$ results in:

$$\frac{L_t}{A}\frac{\partial \dot{m}}{\partial t} = \rho_0 g\beta \oint T\cos\theta ds - \frac{f\dot{m}^2 L_t}{2d\rho_o A^2} \tag{3}$$

The conservation of energy for the different components of the loop is given by,

$$\text{Heater:}\quad \frac{\partial T}{\partial t} + \frac{\dot{m}}{\rho_o A}\frac{\partial T}{\partial s} = \frac{Q}{L_H A \rho_o c_p} \tag{4}$$

$$\text{Cooler:}\quad \frac{\partial T}{\partial t} + \frac{\dot{m}}{\rho_o A}\frac{\partial T}{\partial s} = \frac{-4h(T - T_0)}{d\rho_o c_p} \tag{5}$$

$$\text{Hot and Cold leg:}\quad \frac{\partial T}{\partial t} + \frac{\dot{m}}{\rho_o A}\frac{\partial T}{\partial s} = 0 \tag{6}$$

2.2. Heat transfer and friction factor correlations

The temporal development of the flow regime in this loop depends on the geometrical and heating input power. The fluid is initially at rest and starts to move as soon as heating and cooling are activated. The flow regime may be laminar, transition and turbulent flow in the loop depending on the input power. Hence it is required to deduce a friction factor that smoothly adapts to the continuing change of flow regime. In the present analysis, the well-established friction factor correlation given by Swapnalee and Vijayan [30] has been used for all flow regimes. Maximum of ($f_{laminar} f_{transition} f_{turbulent}$) friction factor employed to adapt smooth transition from laminar to transition and transition to a turbulent regime.

Friction factor for laminar, transition and turbulent flow is given by respectively [30]:

$$f_{la\,min\,ar} = 64/\mathrm{Re} \tag{7}$$

$$f_{transition} = 1.2063/\mathrm{Re}^{0.416} \tag{8}$$

$$f_{turbulent} = 0.316/\mathrm{Re}^{0.25} \tag{9}$$

The entire loop is assumed to be in laminar, transition or turbulent regime depending on the input power. Therefore, to obtain the required Nusselt number in the cooler for solving Eq. (5) at different flow regimes the following correlations are used:

Laminar flow of water:

$$\text{Developing}\quad Nu = 1.86\mathrm{Re}^{(1/3)}\mathrm{Pr}^{(1/3)}(d/L_C)^{(1/3)} \text{ for } \mathrm{Gz} > 10 \tag{10}$$

$$\text{Fully developed (isothermal)}\quad Nu = \frac{hd}{k_f} = 3.66 \text{ for } \mathrm{Gz} \le 10 \tag{11}$$

where, $Gz = (\pi d/4L_C)\mathrm{RePr}$

Transition and turbulent flow of water:

The entry length for the turbulent flow is small, so, it is reasonable to apply the correlation for the transition and turbulent flow given by Gnielinski [31].

$$Nu = 0.012(\mathrm{Re}^{0.87} - 280)\,\mathrm{Pr}^{0.4} \tag{12}$$

Valid for $1.5 < Pr < 500$, $3000 \le Re \le 10^6$.

The nusselt number for laminar flow of hybrid nanofluids in developing the region in the tube is given by Moraveji et al. [32],

$$Nu_{hnf} = 2.03 Re_{hnf}^{0.293}\mathrm{Pr}_{hnf}^{0.6}\phi^{0.06}(d/L_c)^{0.37} \tag{13}$$

Valid for $Re < 2500$ and $0 \le \phi \le 0.06$.

The nusselt number for transition and turbulent flow of hybrid nanofluids in the tube is given by Vijjha et al. [33],

$$Nu_{hnf} = 0.065(Re_{hnf}^{0.65} - 60.22)(1 + 0.0169\phi^{0.15})\mathrm{Pr}_{hnf}^{0.542} \tag{14}$$

valid for $3000 < Re < 16{,}000$ and $0 < \phi < 0.1$; where, $\mathrm{Re}_{hnf} = \frac{\dot{m}_{hnf} d}{\mu_{hnf} A}$, $\mathrm{Pr}_{hnf} = \frac{\mu_{hnf} c_{phnf}}{k_{hnf}}$

2.3. Computation of thermophysical properties of hybrid nanofluids

The properties of hybrid nanofluids like density, coefficient of thermal expansion and specific heat depend on the volume concentration of nanoparticle and their individual properties (Table 1 [34–38]). Therefore, the properties of hybrid nanofluids are calculated by using the mixture model [39] as follows:

$$\rho_{hnf} = \phi_1\rho_1 + \phi_2\rho_2 + (1 - \phi_1 - \phi_2)\rho_f \tag{15}$$

$$(\rho\beta)_{hnf} = \phi_1(\rho\beta)_1 + \phi_2(\rho\beta)_2 + (1 - \phi_1 - \phi_2)(\rho\beta)_f \tag{16}$$

Table 1
Thermophysical properties of nanoparticles and water [31–35].

Thermophysical property	Water	Ag (Spherical)	Cu (Spherical)	Graphene (platelets)	Al_2O_3 (Spherical)	TiO_2 (Spherical)	CNT (Cylindrical)
$\rho(kg/m^3)$	997.1	10,500	8933	2200	3970	4250	2100
$C_p(J/kgK)$	4179	235	385	790	765	686.2	410
$k(W/mK)$	0.613	429	400	5000	40	8.9538	3007.4
$\beta(K^{-1})$	0.00021	0.000054	0.000051	−0.000008	0.000024	0.000024	0.00002

$$(\rho C_p)_{hnf} = \phi_1(\rho C_p)_1 + \phi_2(\rho C_p)_2 + (1-\phi_1-\phi_2)(\rho C_p)_f \quad (17)$$

The transport properties of hybrid nanofluid like thermal conductivity and dynamic viscosity depend on volumetric concentration, their individual properties and the shape (cylindrical, spherical and platelets) of nanoparticles, and hence their influences have been considered for property estimation in this analysis.

Thermal conductivity of nanofluid having nanoparticles of different shapes are calculated with the Hamilton–Crosser model [40] as follows:

$$\frac{k_{nf}}{k_f} = \frac{k_p + (n-1)k_f + (n-1)\phi(k_p - k_f)}{k_p + (n-1)k_f - \phi(k_p - k_f)} \quad (18)$$

where, $n = \frac{3}{\psi}$, n = empirical shape factor, ψ= Sphericity.

Likewise, the viscosity of nanofluid having nanoparticles of different shapes is given by [40],

$$\mu_{nf} = \mu_f(1 + B\phi + C\phi^2) \quad (19)$$

where, B and C are viscosity enhancement coefficient. These are summarized in Table 2.

Dynamic viscosity and thermal conductivity of hybrid nanofluids having nanoparticles of different compositions and shapes have been calculated by using an interpolation method [41]. Hence, the effective dynamic viscosity and thermal conductivity of a hybrid nanofluid with n different types of nanoparticles are calculated by,

$$\mu_{hnf} = \frac{1}{\phi}\sum_{i=1}^{n}(\phi_i\mu_{nf,i}) \text{ where } \phi = \sum_{i=1}^{n}\phi_i \quad (20)$$

$$k_{hnf} = \frac{1}{\phi}\sum_{i=1}^{n}(\phi_i k_{nf,i}) \quad (21)$$

where, ϕ_i, $\mu_{nf,\,i}$ and $k_{nf,\,i}$ are volume concentration, dynamic viscosity (Eq. (19)) and thermal conductivity (Eq. (18)) of i^{th} nanoparticle type. In this study, binary hybrid nanofluids have been used and hence, $n = 2$. It may be noted that n = 3 for tri-hybrid nanofluid and so on.

2.4. Method of solution and energy- exergy performance parameter

The solution of the coupled equations is computed by using the finite difference method (FDM). The transient term in the energy and momentum equation is discretized by using implicit forward Euler form. The first-order upwind discretization is used for the temperature convection term. The discretized equations have been solved by Engineering Equation Solver [42]. Effectiveness is the ratio of actual heat transfer to the maximum possible heat transfer through the cooler. It is the non-dimensional factor, which predicts the enhancement of heat transfer. Transient effectiveness is used for characterizing the dynamic behavior of a heat exchanger and is given by,

$$\varepsilon(t) = \frac{T_{C,in}(t) - T_{C,out}(t)}{T_{C,in}(t) - T_0} \quad (22)$$

In order to analyze the exergetic performance of the single Phase NCL, the entropy generation in the loop has been calculated by using the entropy balance principle. The transient entropy generation rate can be calculated for source (heater), sink (cooler) and adiabatic leg is given, respectively,

$$S_{gen,H}(t) = \dot{m}(t)\left[c_p \ln\left(\frac{T_{H,out}(t)}{T_{H,in}(t)}\right) + \frac{f(t)L_H\dot{m}(t)^2}{2d\rho_{H,avg}^2(t)A^2T_{H,avg}(t)} - \frac{c_p(T_{H,out}(t) - T_{H,in}(t))}{T_{wall,H}(t)}\right] \quad (23)$$

$$S_{gen,C}(t) = \dot{m}(t)\left[c_p \ln\left(\frac{T_{C,out}(t)}{T_{C,in}(t)}\right) + \frac{f(t)L_C\dot{m}(t)^2}{2d\rho_{C,avg}^2(t)A^2T_{C,avg}(t)} - \frac{c_p(T_{C,out}(t) - T_{C,in}(t))}{T_0}\right] \quad (24)$$

$$S_{gen,leg}(t) = \frac{f(t)\dot{m}(t)^3}{2dA^2}\left[\frac{L_{hot,leg}}{\rho_{h,avg}^2(t)T_{h,avg},(t)} + \frac{L_{cold,leg}}{\rho_{c,avg}^2(t)T_{c,avg}(t)}\right] \quad (25)$$

So, the total entropy generation rate in the loop is calculated by,

$$S_{gen,t}(t) = S_{gen,H}(t) + S_{gen,C}(t) + S_{gen,leg}(t) \quad (26)$$

Under steady-state condition.

$T_{H,out}$,$T_{C,in}$ and $T_{h,avg}$ = T_h

$T_{H,in}$,$T_{C,out}$ and $T_{c,avg}$ = $T_c$where, $T_{H,in}$, $T_{H,out}$ and $T_{C,in}$, $T_{C,out}$ are the inlet and outlet temperatures of primary fluid in the heater and cooler respectively.

$T_{H,avg}$, $T_{C,avg}$, $T_{h,avg}$, and $T_{c,avg}$ are the average temperatures of primary fluid in the heater, cooler, hot and cold leg, respectively.

T_h and T_c are the temperatures of primary fluid in the hot and cold leg, respectively, under steady-state condition.

2.5. Grid and time independence study

Grid and time independence test have been carried out to check the consistency of the obtained result, and to make sure that the spatial and temporal discretization error has the minimum impact on the result. The grid independence test with different mesh sizes of 0.01 m, 0.03 m and 0.05 m at a time step of 0.1 s has been performed. The transient variation of the mass flow rate at 500 W has been shown in Fig. 2, which reveals the differences are negligible by increasing the grid size from 0.01 to 0.03 m. Therefore, the optimal grid size of 0.03 m is considered for the subsequent analysis. The time-step independence study has been carried with different sizes of 0.05 s, 0.1 s, 0.5 s and 1 s with the finalized grid size of 0.03 m. Fig. 3 depicts the temporal variation of the mass flow rate at an input power of 500 W. This shows that the calculated mass flow rate remains practically the same with the reduction of time-step from 0.1 s to 0.05 s. Hence, the time-step size of 0.1 s is selected for further analysis.

2.6. Validation of transient and steady-state solution

The numerically obtained data for the transient and steady-state simulations have been compared with the measured values by Vijayan et al. [20] for VHHC orientation of NCL with water as primary fluid. The geometric parameters and operation conditions considered for validation are the loop diameter of 26.9 mm, heater length of 730 mm, cooler length of 800 mm, loop height of 2200 mm, length of bottom leg as 1415 mm, and the inlet temperature of coolant as 304 K. The measured pressure difference at the bottom leg over a length of 1065 mm has been used for validation. Fig. 4 (a, b, c) illustrate the temporal variation of pressure drop (ΔP) at the bottom leg at the different input powers of 232, 368 and 530 W. Assessment of the same reveals the temporal shift of computed values with respect to the measurement. The differences between computed and measured pressure drop after 800 s is < 0.05 mm of the water column and that of the local maximum at about 150–200 s is < 0.025 mm of the water column. The instantons features, such as sudden rise and fall in pressure-drop are captured in the reported analyses. Also, the overall trend is reproduced by the adopted numerical approach. Figs. 5 and 6 show the comparison between the numerical and measured mass flow rate and loop average temperature (T_{avg}) of primary fluid with the at the steady-state. The

Table 2
Sphericity, Empirical shape factor and viscosity enhancement coefficient of different shape of nanoparticle [37].

Nanoparticle shape	Sphericity (ψ)	Empirical shape factor (n)	B	C
Spherical	1	3	2.5	6.2
Cylindrical	0.6122	4.9	13.5	904.4
platelets	0.52	5.7	37.1	612.6

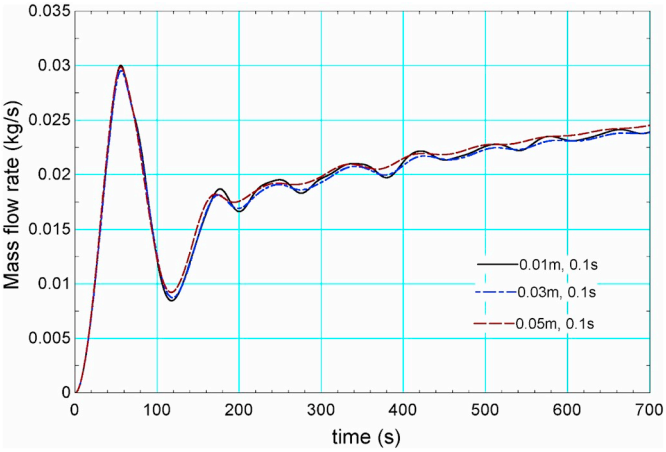

Fig. 2. Temporal variation of mass flow rate for different grid size at time step $\Delta t = 0.1$ s.

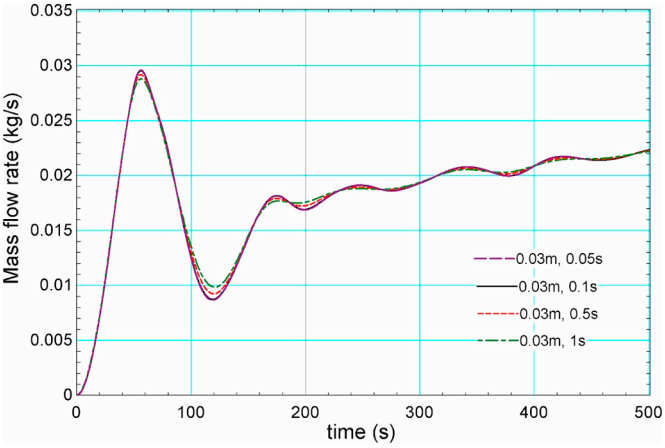

Fig. 3. Temporal variation of mass flow rate for different time step at grid size = .03 m.

average deviation for mass flow rate and T_{avg} at the steady-state is 8.8% and 9.6%, respectively, which is reasonable considering the one-dimensional approach.

3. Results and discussion

The transient and steady-state behavior of VHHC SPNCL has been carried out for different water-based hybrid nanofluids (Al_2O_3 + Ag, Al_2O_3 + Cu, Al_2O_3 + TiO_2, Al_2O_3 + CNT, Al_2O_3 + Graphene), heater power, diameter and loop height. In the simulation, 1% volume concentration of nanoparticle is considered for the transient analysis, which has been reported as an approximate optimum volume concentration for heat transfer applications [43]. The geometric and operating conditions of the loop are given in Table 3.

3.1. Flow initiation in VHHC single phase NCL

The temporal evolution of mass flow rate and spatio-temporal evolution of temperature from no flow condition to the steady-state has been shown in Fig. 7 at a given power of 100 W for water. Initially, the loop fluid was at stagnant condition having temperature equal to the coolant temperature. As soon as heating is activated the primary fluid temperature in the heater increases up to 303 K at an instant given by $t = 25$ s. At the same instant, the entire loop is almost at the initial temperature a strong change between the heater and the connecting hot leg portion. The temperature of the remaining fluid remains unchanged.

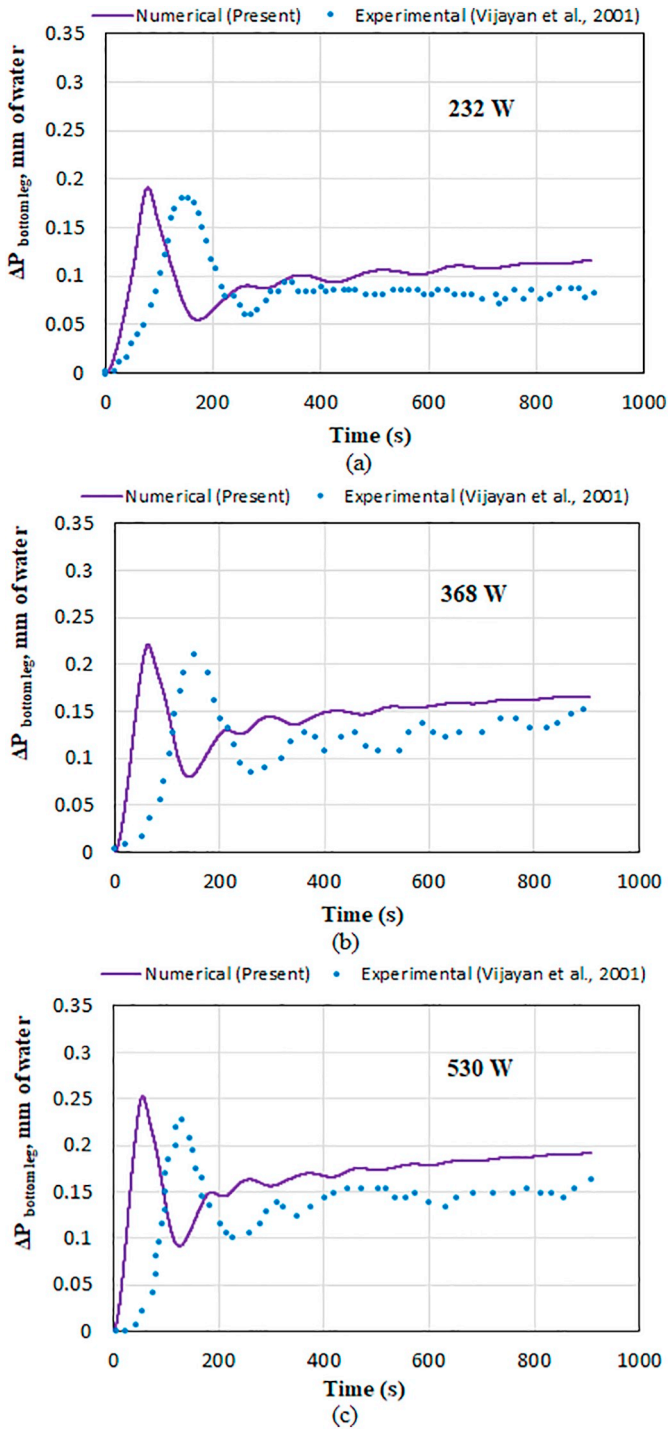

Fig. 4. Temporal pressure drop at the bottom leg of the VHHC at (a) 232 W (b) 368 W and (c) 530 W [20].

This is due to an inadequate buoyancy to overcome the friction loss. As time progresses with a constant power input the buoyancy force exceeds the frictional resistance. This results in setting up natural convection in the loop and the hot-plug moves upward and the heater is occupied with cold water. The mass flow rate reaches the maximum at an instant $t = 100$ s. At this instant the hot-plug shifts towards the cooler. After that the flow is retarded up to $t = 200$ s, the hot-plug enters the top leg in which the cooler is mounted and the buoyancy reduces as the hot leg is filled with relatively cold fluid. Again, at t = 200 s the hot-plug is formed and moved upward as a result sudden increment in the mass flow rate, but this time the temperature of the

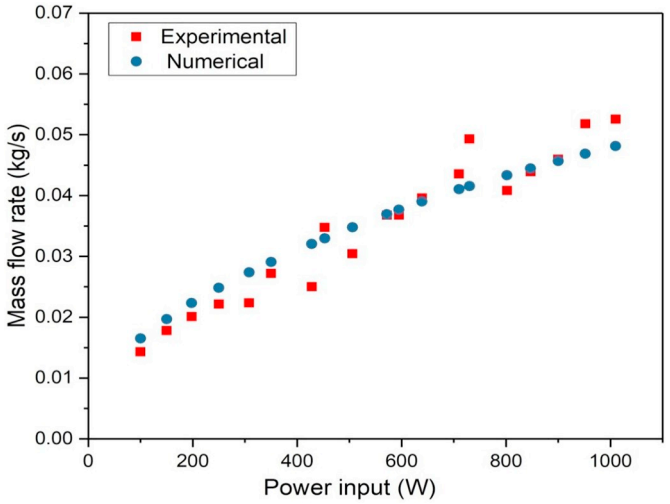

Fig. 5. Comparison of mass flow rate of numerical result with experimental data [20].

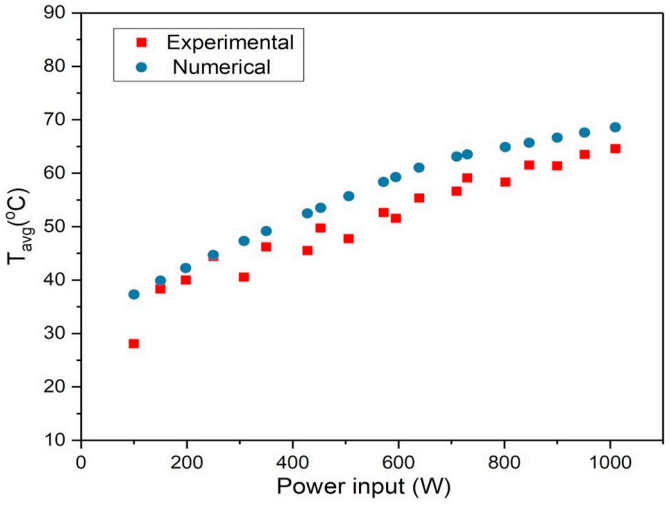

Fig. 6. Comparison of numerical loop average temperature with experimental data [20].

Table 3
Operating condition and geometric parameter used in the present study.

Input Parameters	Values
Loop diameter (internal)	20, 25, 30 mm
Loop Height	1.4, 2.2, 3 m
Loop width	1.415 m
Heating length	0.73 m
Cooling length	0.80 m
Coolant Inlet temperature	301 K
Power input	100, 500, 1000 W
Total nanoparticle concentration	ϕ = 1%

hot-plug is lesser than the previous one because flow is started so fluid is getting less time to heat in the heater. This process will continue till the buoyancy force balances the frictional force and at that time, the steady-state reaches. At t = 2000s, the steady-state condition has been reached; under this condition, the cold leg and hot leg temperatures become the inlet temperature for heater and cooler respectively.

3.2. Transient behavior NCL with water and hybrid nanofluids

The transient variation of mass flow rate in single-phase NCL with

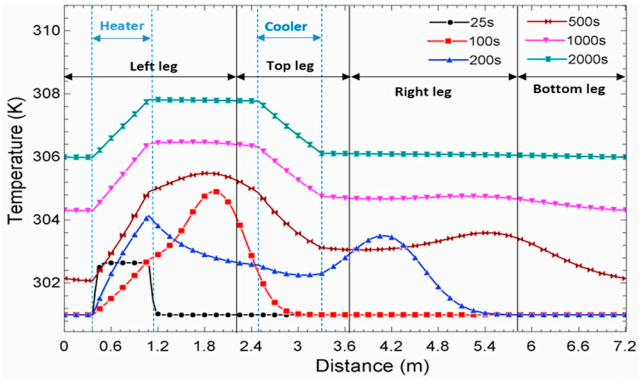

(a)

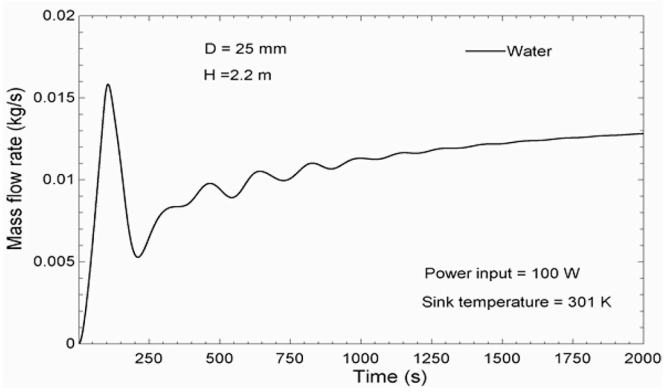

(b)

Fig. 7. Variation of primary fluid (a) temperature along the loop at various instant of time (b) Temporal mass flow rate.

water and different hybrid nanofluids is illustrated in Fig. 8. This reveals the oscillatory nature of the mass flow rate up to 500 s that eventually stabilizes for both the water and hybrid nanofluids. The decay in oscillation indicates the setting up of natural convection and that the flow rate attains a particular value as a consequence of the balance between buoyancy and frictional forces. Detailed analysis reveals the development of hot-plug in the heater with the initiation of heat input. Subsequently, the established temperature difference between adiabatic hot and cold leg overcomes the frictional force leading a sudden increase in the mass flow rate at about 56 s and as the flow rate establishes the amplitude of oscillations decays to a steady flow condition. The amplitude of oscillation is lower for the hybrid

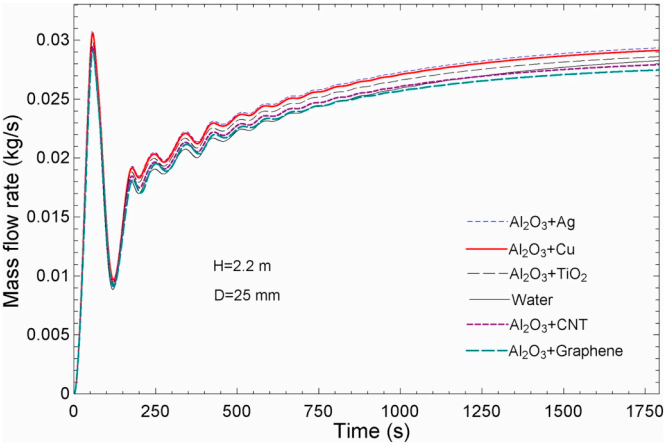

Fig. 8. Temporal variation of mass flow rate of water based hybrid nanofluids at 500 W and 301 K sink temperature.

nanofluids compare to water. The relative maximum amplitudes of oscillation for water, Al_2O_3 + Ag, Al_2O_3 + Cu, Al_2O_3 + TiO_2, Al_2O_3 + CNT, Al_2O_3 + Graphene are 70%, 67%, 68%, 68.44%, 68.5% and 68.6%, respectively. These are quite comparable; however, the time required to attain the steady-state reduces from 1002 s for water to 826 s for Al_2O_3 + Graphene. This is certainly an advantage considering its application in cooling of nuclear reactors wherein this may mitigate the risk of severe accident to certain extent. The relative increase in mass flow rate under steady-state is highest for Al_2O_3 + Ag (3%) followed by Al_2O_3 + Cu (2.8%), Al_2O_3 + TiO_2 (0.5%), While the reduction in mass flow rate is observed for Al_2O_3 + CNT (2.4%) and Al_2O_3 + Graphene (4.1%) compared to water. This is attributed to the increasing buoyancy force with density, temperature difference between adiabatic legs (decreasing specific heat) and thermal expansion coefficient for hybrid nanofluids. On the other hand, the friction loss increases with viscosity and density. Adding nanoparticles in water increases viscosity and density that leads to enhancement in friction force. Therefore, the increase or reduction in mass flow rate of hybrid nanofluids compared to water depends on the net change in buoyancy force and friction force. The dominance of the buoyancy force enhances the mass flow rate while the dominance of the viscous force reduces the mass flow rate. Fig. 8 also illustrates that the steady-state mass flow rate with hybrid nanofluids having spherical shape (Al_2O_3 + Ag, Al_2O_3 + Cu, Al_2O_3 + TiO_2) is higher than that of cylindrical (Al_2O_3 + CNT) and platelets shape (Al_2O_3 + Graphene). These clearly show that the shape and properties of nanoparticles influence the mass flow rate. The lower mass flow rate of hybrid nanofluids having platelets shape (Al_2O_3 + Graphene) and cylindrical shape (Al_2O_3 + CNT) is consistent with high viscosity. A high viscosity may be attributed to the large surface area to volume ratio of nanoparticles. More surface area increases the friction among nanoparticle and fluid particles, which increases the viscosity and hence increases in frictional force; as a result, a decrease in mass flow rate. This indicates that the nanoparticle shape has very significant influence on the performance of SPNCL.

Fig. 9 shows the oscillatory nature of effectiveness that reaches a constant value at the steady-state for both water and hybrid nanofluids. The possible reason behind this oscillatory nature is the initiation of flow as soon the heating is applied on the vertical leg (Fig. 8). This takes certain time to stabilize as a consequence of buoyancy and pressure-drop. Furthermore, the hot fluid takes about 110 s to reach the outlet of horizontal cooler. Thus, the outlet temperature of the cooler ($T_{c,out}$) is the same as coolant temperature (T_0) until 110 s. Therefore, the effectiveness of cooler is unity until the hot fluid passes once through the cooler section at about 110 s as shown in Fig. 9. After t = 110 s the decrease in effectiveness is a consequence of the increase in mass flow rate, which limits the resident time of hot fluid in the cooler section. Again, the effectiveness increases as the mass flow rate of the primary fluid decreases. This oscillatory behavior is stabilized when the flow reaches the steady-state. The relative increase in effectiveness is the highest for Al_2O_3 + Graphene (25.4%) followed by Al_2O_3 + CNT (20.9%), Al_2O_3 + TiO_2 (15.8%), Al_2O_3 + Cu (15.3%) and Al_2O_3 + Ag (15.1%) compare to water.

Fig. 10 depicts that the total entropy generation rate increases with time, which is attributed to the irreversibility at a given power input of 500 W and pressure drop. The increasing mass flow rate or the heat transfer rate with time enhances the associated irreversibility and hence the entropy generation. The internal irreversibility due to the pressure drop also increases that contributes to the overall increase in entropy generation. Fig. 10 also demonstrates that the total entropy generation for all the hybrid nanofluids is less than water. The relative reduction in entropy generation is the highest for Al_2O_3 + Graphene (14.3%) followed by Al_2O_3 + CNT (12.5%), Al_2O_3 + TiO_2 (10.2%), Al_2O_3 + Cu (9.75%) and Al_2O_3 + Ag (9.4%). The possible reason is that under steady-state at specified power input, the entropy generation rate depends on the heater wall temperature, pressure drop and temperature ratio (TR = T_h/T_c). Entropy generation increases with heater wall temperature, TR and pressure drop. The temperature ratio is higher for hybrid nanofluids (due to rise in temperature difference (T_h−T_c)), which increases the entropy generation rate. Due to a high heat transfer coefficient, a low wall temperature for the heater with hybrid nanofluids causes a reduction in entropy generation. Thus, it may be inferred from the analysis that the contribution of pressure drop in the entropy generation is rather small in comparison to the rate of heat input. The resulting increase of TR value and decrease in heater wall temperature shows an adverse effect on entropy generation. Therefore, the net change in entropy generation depends on the dominance of TR value and heater wall temperature. It may be safely stated that the total entropy generation with the hybrid nanofluids is lower in comparison to water. The analysis demonstrates that the hybrid nanofluids have a better energy/entropy performance compare to the base fluid. Al_2O_3 + Ag has higher effectiveness and mass flow rate and lower entropy generation compared to water; hence the forgoing results are based on Al_2O_3 + Ag hybrid nanofluid.

3.3. Effect of heat input rate

The performed simulations are based on the Boussinesq approximation, which is valid for $\beta_{avg}(T\text{-}T_0) \ll 1$. This currently limits the maximum power input to 1000 W at which the maximum temperature difference (T_h-T_0) is about 40 °C and the corresponding change in density is < 2%. Fig. 11 depicts the increasing mass flow rate with heat input, which is attributed to the resulting buoyancy force due to the elevated temperature difference between adiabatic legs. Obviously, at a high heat input rate the flow stabilizes at an early instant of time, which seems to be constant with the findings of Creveling et al. [4]. Fig. 12 illustrates that the heat transfer effectiveness reduces with the increasing power input as a consequence of the enhanced mass flow rate that reduces the available cooling or heat removal time. Therefore, the denominator term in effectiveness Eq. (22) increases. Since both the numerator and denominator terms are increasing with the heating power, so the net effect depends on their rate of change. This can also be inferred from the amplitude of mass flow rate oscillations with input power in Fig. 11. Obviously, with the increasing input power the corresponding rise in mass flow rate results in faster decay of effectiveness in comparison to the lowest input power (Fig. 12). Fig. 13 demonstrates that the entropy generation rate is higher for higher heater power. This is due to the fact that the entropy generation increases due to irreversibility associated with pressure drop and heat transfer rate. So, increasing heater power increases heat transfer rate and pressure drop, which increases irreversibility associated with it, resulting in increase

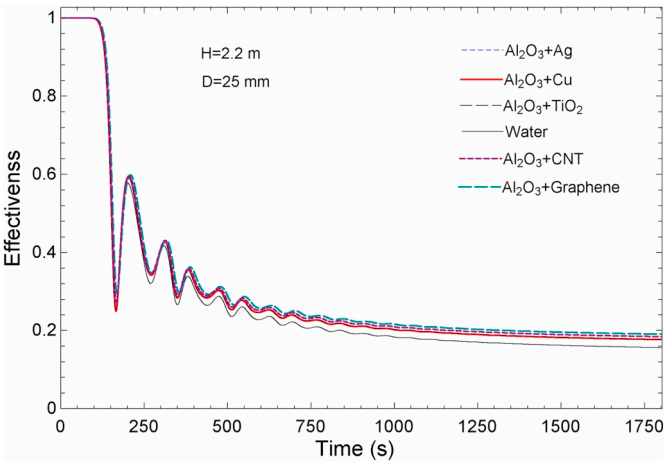

Fig. 9. Temporal variation of effectiveness of water based hybrid nanofluids at 500 W and 301 K sink temperature.

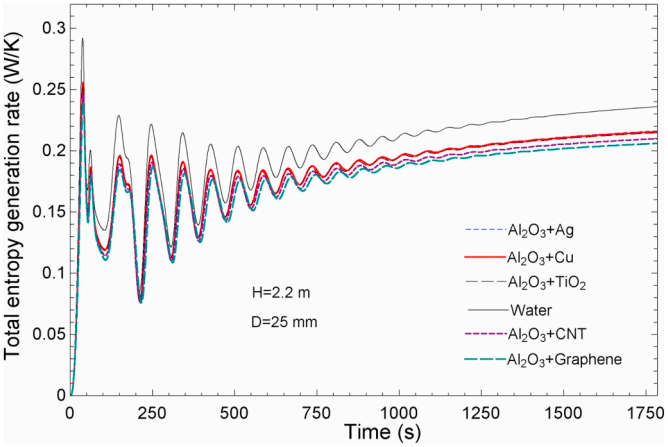

Fig. 10. Temporal response of total entropy generation rate of hybrid nanofluids at 500 W and 301 K sink temperature.

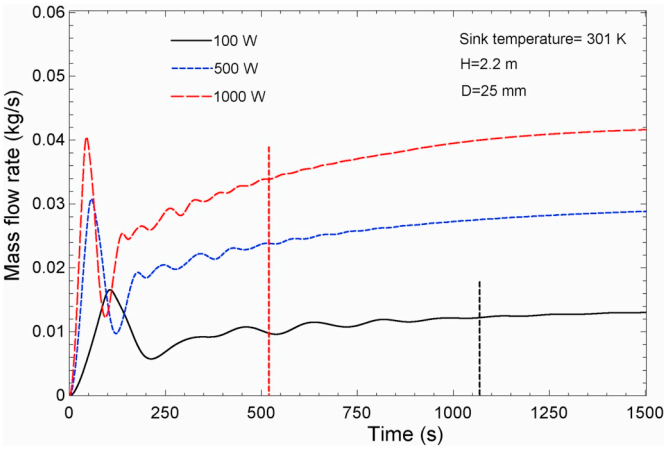

Fig. 11. Influence of various heater power on the temporal variation of mass flow rate for Al_2O_3 + Ag hybrid nanofluid.

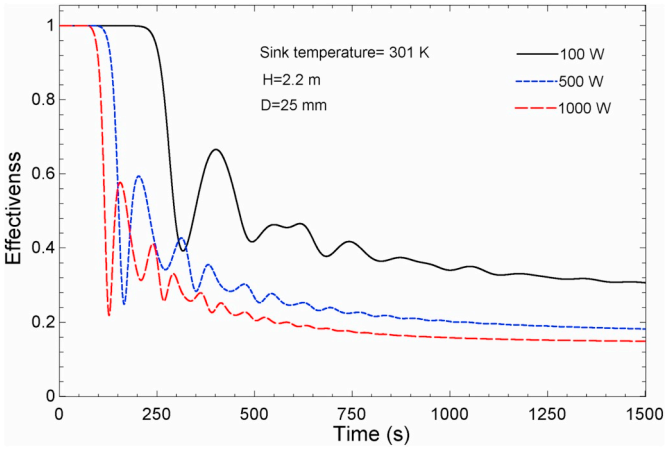

Fig. 12. Influence of heater power on temporal effectiveness for Al_2O_3 + Ag hybrid nanofluid.

in entropy generation.

3.4. Effect of geometric properties

In this segment, the influence of the diameter and height of the loop on the different performance parameters have been presented. Fig. 14 demonstrates that the amplitude of fluctuation of mass flow rate and time required to reach the steady-state is the least for the smallest diameter of tube. A possible reason is the increasing friction or viscous effect with the decreasing tube diameter at a given mass flow rate, which is consistent with the findings of Vijayan et al. [8]. This figure also illustrates that increasing the tube diameter increases the mass flow rate at a given input power, which is obvious from the reduced friction to the fluid flow that varies inversely with tube diameter.

Fig. 15 illustrates that decreasing the tube diameter enhances the steady-state effectiveness of single-phase NCL. This is attributed to the decrease in mass flow rate by virtue of the offered flow resistance that rises the temperature difference (T_h−T_c). The heat transfer coefficient is directly proportional to $Re^m \times Pr^n$ and therefore, it varies inversely with pipe diameter$^{(1-m)}$. The value of m is < 1, hence the heat transfer coefficient varies inversely with tube diameter. Therefore, decreasing the tube diameter increases the heat transfer coefficient, which reduces the temperature difference (T_h-T_0); as a result, enhancement in effectiveness. The effectiveness remains unity until 110 s at 500 W, which may be attributed to the comparable mass flow rates at 110 s at the selected marginally different diameters.

Fig. 16 illustrates that reducing the tube diameter increases the entropy generation of NCL. The possible reason is that a reduction in the mass flow rate with smaller tube diameter rises the hot and cold leg temperature difference and thus temperature ratio, resulting in increase in entropy generation. The heater wall temperature also increases leading to the enhancement in entropy generation.

Fig. 17 illustrates the influence of height of loop on the temporal variation of mass flow rate in NCL. This reveals that the highest fluctuations of mass flow rate and time required to achieve the steady state correspond to the height of loop. Furthermore, as a consequence of the buoyancy, the steady state mass flow rate increases with the height at a specified power input of 500 W. However, the pressure drop also increases as a result of loop length corresponding to its height. Thus, the counter effect of buoyancy and pressure drop reduces the relative increase in mass flow rate as the loop height is increased. Fig. 18 illustrates that the increasing the loop height reduces the steady state effectiveness of the cooler. This may be explained by the fact that increasing the height increases the mass flow rate and decreases the temperature difference (T_h−T_c). The increase in heat transfer coefficient (because of increased mass flow rate) decreases the temperature difference (T_h-T_0). Since both temperature differences are decreasing so the net effect is dependent on their rate of decrement. As expected, the reduction in the loop height results in an early reduction of effectiveness from unity at a given input power. Fig. 19 illustrates that the steady state entropy generation reduces with raising the height of the loop. This is because of the increasing loop height enhances the mass flow rate, which increases the heat transfer coefficient and hence

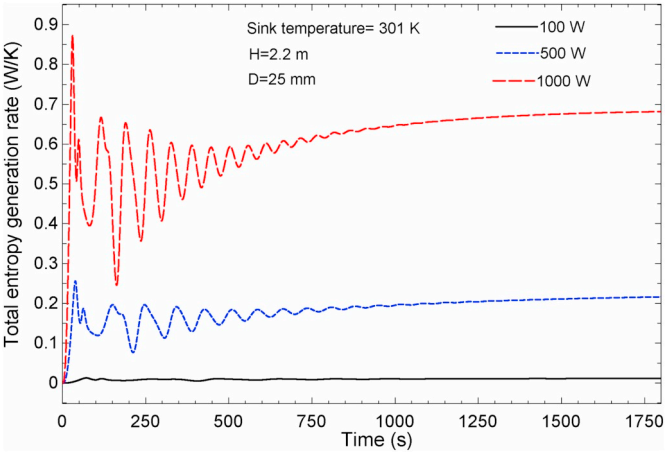

Fig. 13. Effect of heater power on total entropy generation rate for Al_2O_3 + Ag hybrid nanofluid.

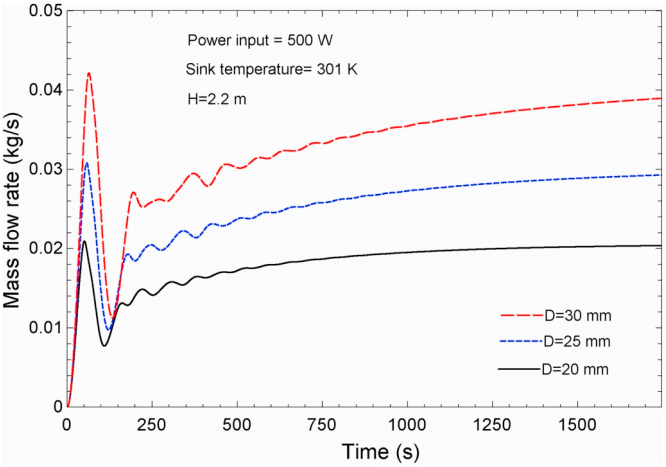

Fig. 14. Influence of loop diameter on the temporal variation of mass flow rate for Al_2O_3 + Ag hybrid nanofluid.

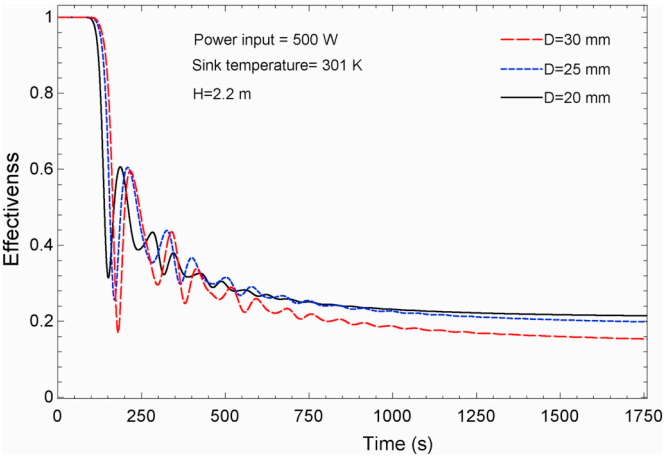

Fig. 15. Influence of loop diameter on the temporal variation of effectiveness for Al_2O_3 + Ag hybrid nanofluid.

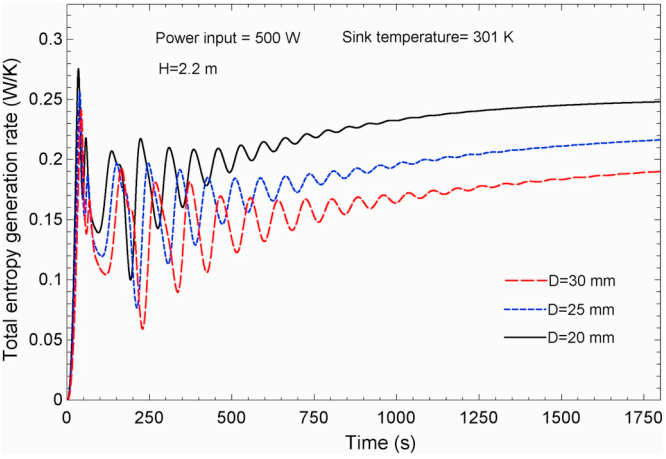

Fig. 16. Influence of loop diameter on the temporal variation of total entropy generation for Al_2O_3 + Ag hybrid nanofluid.

decreases the temperature difference for heat transfer resulting reduction in the entropy generation. Also, increasing height extends the total loop length and mass flow rate, which results in increment in the pressure drop. So, the irreversibility associated with pressure drop

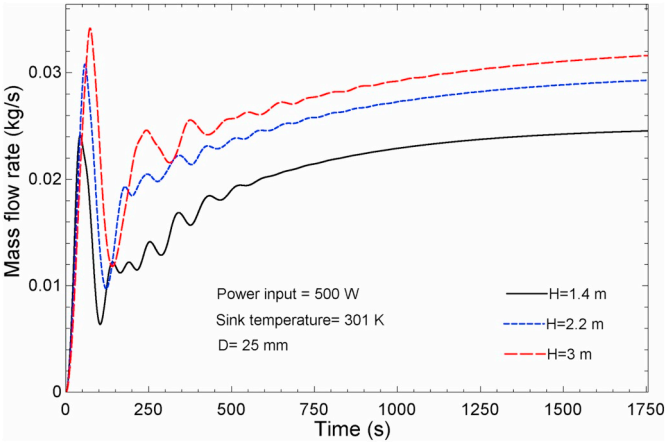

Fig. 17. Influence of loop height on the temporal variation of mass flow rate for Al_2O_3 + Ag hybrid nanofluid.

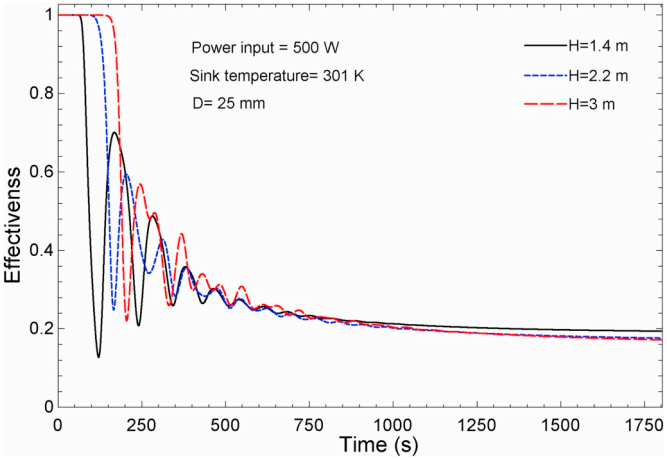

Fig. 18. Influence of loop height on temporal effectiveness for Al_2O_3 + Ag hybrid nanofluid.

increases, causing increase in entropy generation. However, the entropy generation caused by pressure drop is negligible of the order 10^{-6}. Hence increasing the height of the loop reduce total entropy generation of NCL.

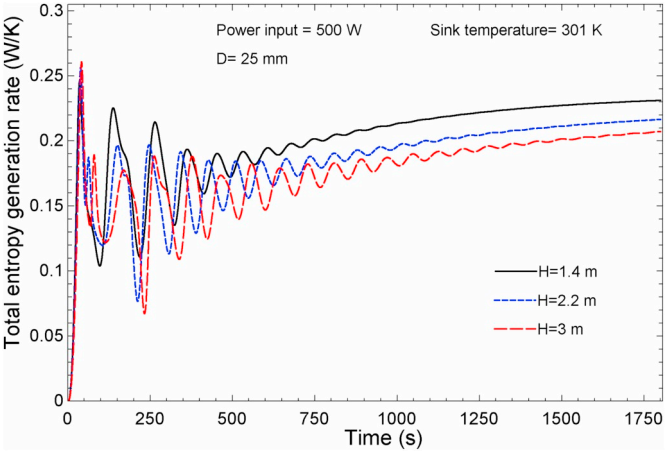

Fig. 19. Influence of loop height on entropy generation for Al_2O_3 + Ag hybrid nanofluid.

4. Conclusions

This study investigates the transient behavior of a vertical heating and horizontal cooling based rectangular Single-phase NCL with water and water-based hybrid nanofluids having a volume concentration of 1%. The influence of different hybrid nanofluids, power input, tube diameter and loop height on the performance parameter such as, effectiveness, total entropy generation and mass flow rate are analyzed. The major findings are:

a) The hybrid nanofluids mitigate the instability, which is inferred from the amplitude of mass flow rate oscillations with respect to water-based natural circulation loop.
b) The time required to attain a steady-state is reduced with hybrid nanofluids than water at a given power input. This is definitely beneficial for system wherein heat removal rate is a major concern and steady-state is desired. Moreover, the shape and type of nanoparticles influence the transient behavior of SPNCL.
c) The mass flow rate for hybrid nanofluids with the spherical nanoparticles (Al_2O_3 + Ag, Al_2O_3 + Cu, Al_2O_3 + TiO_2) is higher as compared to water. Whereas, the mass flow rate of hybrid nanofluids with cylindrical (Al_2O_3 + CNT) and platelets (Al_2O_3 + Graphene) shaped particle is lower than water and spherical nanoparticle dispersed hybrid nanofluids.
d) Higher effectiveness and a lower total entropy generation are achievable with hybrid nanofluids as compared to water.
e) The time required to achieve a steady-state is less for higher power input. Whereas, the steady mass flow rate and total entropy generation increase, and effectiveness decreases with increasing power input.
f) The effectiveness of cooler remains unity until the hot fluid passes once through this device. Increasing power input results in an early drop in effectiveness from unity. The marginal change in loop diameter does not affect this parameter significantly at a given input power.
g) The mass flow rate and its fluctuation along with the time required to achieve a steady-state increase with tube diameter and height. However, the steady total entropy generation and effectiveness reduce with increasing loop height and tube diameter.

Declaration of Competing Interest

There is no conflict of interest for this article.

References

[1] Y. Zvirin, A review of N. C. loops in PWR and other systems, Nucl. Eng. Des. 67 (1981) 203–225.
[2] A.K. Yadav, S. Bhattacharyya, M. Ramgopal, Optimum operating conditions for subcritical/supercritical fluid-based natural circulation loops, J. Heat Transf. 138 (2016) 112501.
[3] P. Welander, On the oscillatory instability of a differentially heated fluid loop, J. Fluid Mech. 29 (1979) 17–30.
[4] H.F. Creveling, F.Z. De Paz, J.Y. Baladi, J. Schoenhals, Stability characteristics of a single-phase free convection loop, J. Fluid Mech. 67 (1975) 65–84.
[5] K. Chen, On the oscillatory instability of closed loop thermosyphons, J. Heat Transf. 107 (1985) 826–831.
[6] P.K. Vijayan, Experimental observations on the general trends of the steady state and stability behaviour of single-phase natural circulation loops, Nucl. Eng. Des. 215 (2002) 139–152.
[7] S.K. Mousavian, M. Misale, F. D'Auria, M.A. Salehi, Transient and stability analysis in single-phase natural circulation loop, Ann. Nucl. Energy 31 (2004) 1177–1198.
[8] P.K. Vijayan, A.K. Nayak, D. Saha, M.R. Gartia, Effect of loop diameter on the steady state and stability behaviour of single-phase and two-phase natural circulation loops, Sci. Technol. Nuclear Install. 2008 (2008) 672704.
[9] N.M. Rao, M. Mishra, B. Maiti, P.K. Das, Dynamic performance of a natural circulation loop with end heat exchangers under different excitations, Int. Com. Heat Mass Transf. 48 (2005) 3185–3196.
[10] D.N. Basu, S. Bhattacharyya, P.K. Das, Performance comparison of rectangular and toroidal natural circulation loops under steady and transient conditions, Int. J. Therm. Sci. 57 (2012) 142–151.
[11] D.N. Basu, S. Bhattacharyya, P.K. Das, Dynamic response of a single-phase rectangular natural circulation loop to different excitations of input power, Int. J. Heat Mass Transf. 65 (2013) 131–142.
[12] F. Devia, M. Misale, Analysis of the effects of heat sink temperature on single-phase natural circulation loops behaviour, Int. J. Therm. Sci. 59 (2012) 195–202.
[13] M. Misale, Experimental study on the influence of power steps on the thermo-hydraulic behavior of a natural circulation loop, Int. J. Heat Mass Transf. 99 (2016) 782–791.
[14] L. Luzzi, M. Misale, F. Devia, A. Pini, M.T. Cauzzi, F. Fanale, A. Cammi, Assessment of analytical and numerical models on experimental data for the study of single-phase natural circulation dynamics in a vertical loop, Chem. Eng. Sci. 162 (2017) 262–283.
[15] A. Cammi, M. Misale, F. Devia, M.T. Cauzzi, A. Pini, L. Luzzi, Stability analysis by means of information entropy: assessment of a novel method against natural circulation experimental data, Chem. Eng. Sci. 166 (2017) 220–234.
[16] A. Marchitto, M. Misale, Experiments on parallel connected loops in single phase natural circulation: preliminary results, Math. Model.Eng. Probl. 5 (2018) 161–167.
[17] A.K. Srivastava, J.Y. Kudariyawar, A. Borgohain, S.S. Jana, N.K. Maheshwari, P.K. Vijayan, Experimental and theoretical studies on the natural circulation behavior of molten salt loop, Appl. Therm. Eng. 98 (2016) 513–521.
[18] M. Krishnani, D.N. Basu, Computational stability appraisal of rectangular natural circulation loop: effect of loop inclination, Ann. Nucl. Energy 107 (2017) 17–30.
[19] M. Misale, M. Frogheri, Influence of pressure drops on the behavior of a single-phase natural circulation loop: preliminary results, Int. Commun. Heat Mass Transf. 26 (1999) 597–606.
[20] P.K. Vijayan, V.K. Bhojwani, M.H. Bade, M. Sharma, A.K. Nayak, D. Saha, R.K. Sinha, Investigation on the effect of heater and cooler orientation on the steady state, transient and stability behaviour of single-phase natural circulation in a rectangular loop, BARC/2001/E/034, 2002.
[21] M. Misale, P. Garibaldi, L. Tarozzi, G.S. Barozzi, Influence of thermal boundary conditions on the dynamic behaviour of a rectangular single-phase natural circulation loop, Int. J. Heat Fluid Flow 32 (2011) 413–423.
[22] A.K. Nayak, M.R. Gartia, P.K. Vijayan, An experimental investigation of single-phase natural circulation behaviour in a rectangular loop with Al2O3 nanofluids, Exp. Thermal Fluid Sci. 33 (2008) 184–189.
[23] A.K. Nayak, M.R. Gartia, P.K. Vijayan, Thermal–hydraulic characteristics of a single-phase natural circulation loop with water and Al2O3 nanofluid, Nucl. Eng. Des. 239 (2009) 526–540.
[24] M. Misale, F. Devia, P. Garibaldi, Experiments with Al2O3 nanofluid in a single-phase natural circulation mini-loop: preliminary results, Appl. Therm. Eng. 40 (2012) 64–70.
[25] C.J. Ho, Y.N. Chung, C.M. Lai, Thermal performance of Al2O3/water nanofluid in a natural circulation loop with a mini-channel heat sink and heat source, Energy Convers. Manag. 87 (2014) 848–858.
[26] S. Dogana, A. Turgut, Enhanced effectiveness of nanofluid based natural circulation mini loop, Appl. Therm. Eng. 75 (2015) 669–676.
[27] H.D. Koca, S. Doganay, A. Turgut, Thermal characteristics and performance of ag-water nanofluid: application to natural circulation loops, Energy Convers. Manag. 135 (2017) 9–20.
[28] P. Devi, C.S. Rao, K. Kumar, Suitability of magnetic nanofluid in heat transfer loops, Int. J. Heat Technol. 36 (2018) 195–200.
[29] S. Thomas, C.B. Sobhan, Stability and transient performance of vertical heater vertical cooler natural circulation loops with metal oxide nanoparticle suspensions, Heat Transf. Eng. 39 (2018) 861–873.
[30] B.T. Swapnalee, P.K. Vijayan, A generalized flow equation for single phase natural circulation loops obeying multiple friction laws, Int. J. Heat Mass Transf. 54 (2011) 2618–2629.
[31] V. Gnielinski, New equations for heat and mass transfer in turbulent pipe and channel flow, Int. Chem. Eng. 16 (1976) 359–368.
[32] M.K. Moraveji, M. Darabi, S.M.H. Haddad, R. Dabvaranejad, Modelling of convective heat transfer of a nanofluid in the developing region of a tube flow with computational fluid dyanamics, Int. Commun. Heat Mass Transf. 38 (2011) 1291–1295.
[33] R.S. Vijjaha, D.K. Das, Development of new correlations for convective heat transfer and friction factor in turbulent regime for nanofluid, Int. J. Heat Mass Transf. 53 (2010) 4607–4618.
[34] E.B. Ogut, Natural convection of water-based nanofluids in an inclined enclosure with a heat source, Int. J. Therm. Sci. 48 (2009) 2063–2073.
[35] M. Devarajan, N.P. Krishnamurthy, M. Balasubramanian, B. Ramani, S. Wongwises, K.A. El-Naby, R. Sathyamurthy, Thermophysical properties of CNT and CNT/Al2O3 hybrid nanofluid, Micro Nano Lett. 13 (2018) 617–621.
[36] L. Deng, R.J. Young, I.A. Kinloch, R. Sun, G. Zhang, L. Noe, M. Monthioux, Coefficient of thermal expansion of carbon nanotubes measured by Ramaspectroscopy, Appl. Phys. Lett. 104 (2014) 051901.
[37] D. Yoon, Y.W. Son, H. Cheong, Negative thermal expansion coefficient of graphene measured by Raman spectroscopy, Nano Lett. 11 (2011) 3227–3231.
[38] N. Ahammed, L.G. Asirvatham, S. Wongwises, Entropy generation analysis of graphene–alumina hybrid nanofluids in multiport mini channel heat exchanger coupled with thermoelectric cooler, Int. J. Heat Mass Transf. 103 (2016) 1084–1097.
[39] A.J. Chamkha, I.V. Miroshnichenko, M.A. Sheremet, Numerical analysis of unsteady conjugate natural convection of hybrid water-based nanofluid in a semi-circular

cavity, J. Therm. Sci. Eng. Appl. 9 (2017) 1–9.
[40] E.V. Timofeeva, J.L. Routbort, D. Singh, Particle shape effects on thermophysical properties of alumina nanofluids, J. Appl. Phys. 106 (2009) 014304.
[41] M. Sahu, J. Sarkar, Steady state energetic and exergetic performances of single phase natural circulation loop with hybrid nanofluids, J. Heat Transf. 141 (2019) 082401.
[42] S.A. Klein, Engineering equation solver professional, Version V10, 215 F-Chart Software, Madison, WI, 2017.
[43] A.K. Tiwari, P. Ghosh, J. Sarkar, Particle concentration levels of various nanofluids in plate heat exchanger for best performance, Int. J. Heat Mass Transf. 89 (2015) 1110–1118.